

# Tracking quantum clouds expansion in tunneling ionization

I. A. Ivanov<sup>1,2,\*</sup>, A.S.Kheifets<sup>2,†</sup> and Kyung Taec Kim<sup>1,3‡</sup>

<sup>1</sup> *Center for Relativistic Laser Science,*

*Institute for Basic Science (IBS), Gwangju 61005, Republic of Korea*

<sup>2</sup> *Research School of Physics, Australian National University, Canberra ACT 2601, Australia and*

<sup>3</sup>*Department of Physics and Photon Science, GIST, Gwangju 61005, Korea*

(Dated: October 18, 2023)

We study formation and evolution of the electron wave-packets in the process of strong field ionization of various atomic targets. Our study is based on reformulating the problem in terms of conditional amplitudes, i.e., the amplitudes describing outcomes of measurements of different observables provided that the electron is found in the ionized state after the end of the pulse. By choosing the electron coordinate as such an observable, we were able to define unambiguously the notion of the ionized wave-packets and to study their formation and spread. We show that the evolution of the ionized wave packets obtained in this way follows closely the classical trajectories at the initial stages of evolution providing an *ab initio* quantum-mechanical confirmation of the basic premises of the Classical Monte Carlo Calculations approach. At the later stages of evolution the picture becomes more complicated due to the wave packets' spread and due to interference of wave packets originating from different field maxima. Our approach also allowed us to obtain information about the coordinate and velocity electron distributions at the tunnel exit.

## Introduction

The notion of an electron trajectory proved itself extremely useful for the qualitative and, in many cases, quantitative description of various ionization phenomena. Even the simplest

---

\*Electronic address: igorivanov@ibs.re.kr

†Electronic address: A.Kheifets@anu.edu.au

‡Electronic address: kyungtaec@gist.ac.kr

picture of classical electron motion in the field of an electromagnetic wave, the well-known simple man model (SMM) and its predecessors [1–12], provides a basis for understanding many ionization phenomena, such as above-threshold ionization (ATI) and high harmonic generation (HHG). The spectacular predictive power of the SMM gave rise to a variety of techniques in which the ionization is described quantum-mechanically and the subsequent electron motion is treated classically or semi-classically (classical trajectory Monte Carlo or CTMC method) [11–18]. In these approaches the role of quantum-mechanics (QM) consists in setting up initial conditions for the subsequent classical or semi-classical electron motion, and to assigning statistical weights to the trajectories originating at different times by employing the notion of the instantaneous ionization rate (IIR). Various analytical expressions for the IIR obtained in the framework of the quantum-mechanical strong field approximation (SFA) approach and its subsequent developments [19–25] can be used for this purpose, such as the Ammosov-Delone-Krainov (ADK) [24, 26], or the Yudin-Ivanov [27] formulas.

The initial values of the coordinates for the classical trajectories are determined by the tunnel exit position, which can be found using the field direction model (FDM) [17] or a more refined approach based on the use of the parabolic coordinate system [28] for the atomic systems governed purely by the Coulomb interaction. The initial velocities in the directions perpendicular to the orientation of the electric field vector at the time of ionization are typically assumed to be distributed according to the well-known SFA formula for the transverse velocity distribution [23]. The initial velocity in the direction parallel to the electric field vector at the moment of ionization is typically assumed to be zero [18].

The success and utility of this semi-classical picture of atomic and molecular ionization is ultimately due to the essentially semiclassical nature of many aspects of the ionization phenomena which can be explained quite satisfactorily using semiclassical trajectory simulations. The so-called low-energy structures in strong field ionization spectra [29, 30], Coulomb focusing effect [31], nonadiabatic effects in strong field ionization [32], frustrated tunneling ionization [33], have been studied using the trajectory-based methods. The semi-classical approaches based on the classical trajectories can include the interference effects as well, which can be done by using the so-called Quantum Trajectory Monte Carlo (QTMC) approach [34, 35], or the semiclassical two-step model for strong-field ionization [36], which allows to obtain angular photo-electron distributions in good agreement with fully quantum calculations based on the solution of the time-dependent Schrödinger equation (TDSE).

Such semiclassical simulations usually require much less computational effort than the fully quantum calculations and consequently, for complex targets, when numerical solution of the TDSE becomes unfeasible, use of such methods may provide the only possibility to obtain quantitative description of the ionization process.

If we are interested in a purely quantum mechanical description of the motion of ionized electrons and still want to be able to use some classical notions, one can apply the saddle-point method (SPM) to evaluate the SFA [7, 37–42] or the Feynman’s path-integral expressions for the ionization amplitude [43]. One obtains in this way a description of the ionization phenomena in terms of the so-called quantum trajectories (QT). QT are determined by the SPM equations and make the action in the integrals determining ionization amplitudes stationary. QT is a generally complex electron trajectory originating at the complex saddle point  $t_s$  and propagating till the final moment of time  $t_f$ , when the electron arrives at the detector. This approach gives a very transparent and appealing view of the ionization process. It is, moreover, very flexible and allows to design a number of different generalizations and developments [37, 44]. One may, for instance, start with the SFA ionization amplitude, ignoring effects of the ionic potential in the continuum [37, 45, 46], evaluate it applying the SPM [37, 43, 46, 47] and obtain a description of the ionization process in terms of the complex QT which are solutions to Newton’s equations for a classical electron in the presence of the laser field. Such a description provides a link with the SMM. To include the effects of the ionic potential one can consider perturbatively the Coulomb effects on the QT used in the SFA (the so-called Coulomb corrected SFA or CCSFA method [48]). Alternatively, one can consider the Coulomb and laser field effects on the trajectories on equal footing and find the QT as solutions to the Newton’s equations of motion in presence of the Coulomb and laser fields, still using the SFA equation defining the saddle-point (the Trajectory-based Coulomb SFA or (TCSFA) method [49]). Yet more generally, one may apply the SPM to evaluate the Feynman’s path-integral representation of the ionization amplitude [43], obtaining QT which are solutions to the Newton’s equations of motion in presence of the Coulomb and laser fields with a more complicated condition defining the starting time  $t_s$  of the trajectory.

The path connecting  $t_s$  and  $t_f$  in the complex time-plane is often chosen to consist of two straight line segments:  $(t_s, Re\ t_s)$  and  $(Re\ t_s, t_f)$ , with  $Re\ t_s$  interpreted as the tunnel exit point. One should bear in mind, however, that QT are all but a convenient (albeit very

useful and powerful) mathematical construct, arising as a result of the application of the SPM for evaluation of ionization amplitudes. In particular, the path connecting  $t_s$  and  $t_f$  described above is not unique and can be deformed to cross the real time-axis almost at any given point [37]. This remark applies equally, of course, to the notion of the tunnel exit used in the CTMC method [37, 44].

This path-dependence of the time and location of the tunnel exit does not affect the quantum amplitude since the integrals defining the amplitudes depend only on the end points  $t_s$  and  $t_f$  of the path (as long as deforming the path we do not cross singular points of the integrand in the complex time-plane). As it was mentioned in the review work [37], no physical experiment can favor particular values for time or location of the tunnel exit event, which does not prevent these notions to be extremely useful for practical purposes. In practice, the path connecting  $t_s$  and  $t_f$ , consisting of the two straight line segments:  $(t_s, Re t_s)$  and  $(Re t_s, t_f)$  is the most convenient choice. The exit time  $Re t_s$  and the tunnel exit point are related to the corresponding sub-barrier part of the QT as the real part of the expression  $\mathbf{r} = \int_{t_s}^{Re t_s} \mathbf{v}(t) dt$ , where  $\mathbf{v}(t)$  is the complex-valued sub-barrier electron velocity. The sub-barrier part of the QT thus defined can be used to provide the necessary prerequisites for the CTMC simulations, such as position of the tunnel exit, the transverse and longitudinal momentum distributions at the tunnel exit and the instantaneous ionization rate [34, 50]. Taking the real part of the QT at  $t = Re t_s$  as the tunnel exit position has the advantage that the imaginary part of the action which determines the ionization probability is accumulated in the sub-barrier region, while subsequent propagation of the QT in the real time only produces phase-shift due to the change of the real part of the action. This choice also allows to avoid complicated issues of branching points and branch cuts in the complex time-plane [44].

Of course, all the information we can hope to obtain about a physical system is encoded in its wave function. Any question about the motion of the ionized wave-packets for times within the laser pulse, should therefore be resolved from the solution of the TDSE, provided that this question has a physical meaning at all. The approach based solely on the information obtained by solving the TDSE, however, encounters the problem of identifying the contributions from different channels (ionization, excitation, and so on) for times within the laser pulse, when the wave-packets corresponding to these channels are not spatially sepa-

rated yet. The splitting of the total wave-function of the system into the bound and ionized components seems to have been achieved in the SFA and the Perelomov-Popov-Terent'ev (PPT) approaches [19–23, 26]. Such a splitting is not unique, however, and it is different in the two theories. Moreover, it is not gauge-invariant in the SFA or PPT approaches [37]. Similarly, the procedure based on projecting out contributions of the bound states of the field-free atomic Hamiltonian from the TDSE wave-function, which is sometimes used to define wave-packet describing ionized electron, is not gauge-invariant when applied for the times within the laser pulse duration.

In [51] a method, allowing to identify the part of the wave-function describing ionized electron and relating the TDSE-based approach with the insight offered by the trajectory based approaches, has been proposed. In the framework of this method the photoionized part of the wave function is singled out by means of applying the time dependent surface flux (tSURFF) method [52], which relies on the knowledge of the wave-function in the asymptotic region, when the photo-ionized part of the wave function is localized in space. By applying a short-time filter to the ionization amplitude, calculated using the tSURFF method, authors were able to identify the dominant pathways which form the photoelectron spectra.

Another group of methods allowing to connect the TDSE and the notion of trajectory is based on the Bohmian interpretation of the QM [53]. Bohmian view of the QM introduces a well-defined notion of the electron trajectory, exactly reproducing at the same time all the predictions of the conventional QM [54]. This possibility of reintroducing trajectories in the QM framework has been exploited to describe ionization of atoms [55, 56] and molecules [57] driven by strong laser fields, and for the description of the HHG process [58–60]. An approach to the problem of the tunneling time, based on the Bohmian QM, has been described in [61]. In [62] the notion of the coordinate distributions describing ionized electrons has been defined using the Bohmian trajectories, which allowed to look at the tunnel exit problem from the perspective offered by the Bohmian QM.

In our earlier works [63–65] we described an alternative method that allowed us to extract from the TDSE information about the time-development of the ionization process for times within the laser pulse duration. The method is based on the analysis of two-time correlation functions, computed using the time-dependent wave-function describing evolution of the system, which was obtained by solving the TDSE numerically. In essence, this procedure allows us to use the notion of the conditional probability, where the condition is imposed

at an instant when the laser pulse is gone. In other words, we formulate the questions about different observables characterizing the electron motion in the following way: What would be the probability of observing a given value of a certain observable during the laser pulse, provided that the electron is found in a given state at the end of the laser pulse? We applied this technique to study the evolution of the electron velocity distribution in strong field ionization [64] and to study trajectories of the electron wave-packets for the process of the frustrated tunneling ionization (FTI) [65]. Here we report a study of evolution of the ionized wave-packets for the process of strong field ionization, based on the analysis of the information obtained from the numerical solution of the TDSE.

Atomic units with  $\hbar = 1$ ,  $e = 1$ ,  $m = 1$  where  $e$  and  $m$  being the charge and the mass of the electron are used throughout the paper.

### Theory

We consider an atom interacting with a linearly polarized laser pulse which we define in terms of its vector potential:  $\mathbf{E}(t) = -\frac{\partial \mathbf{A}(t)}{\partial t}$ , where:

$$\mathbf{A}(t) = -\hat{e}_z \frac{E_0}{\omega} \sin^2\left(\frac{\pi t}{T_1}\right) \sin(\omega t + \phi) . \quad (1)$$

Here  $T_1 = N_c T$  is the total pulse duration and  $T = 2\pi/\omega$  is the optical cycle (o.c.) corresponding to the central frequency  $\omega = 0.057$  a.u. (the wavelength of 800 nm). In the calculations below we use pulses with  $N_c = 4$ . The target system is described using the single-active electron (SAE) approximation and a spherical potential  $V(r)$ . As targets, we will consider the hydrogen atom with  $V(r) = -1/r$ , a model atom with a short range (SR) Yukawa-type potential  $V(r) = -1.903e^{-r}/r$  and the Ar atom described by means of an effective potential [66]. The target atom is initially in the ground state  $|\phi_0\rangle$ , which is an  $s$  state for the hydrogen and Yukawa atoms (both with the ionization potential of 0.5 a.u.) and a  $p$  state with the energy -0.59 a.u. in the case of the Ar atom.

We have shown in earlier works [63–65] that tunneling ionization dynamics can be studied in detail by analyzing suitably chosen two-time correlation functions:

$$C(A(t_1)B(t_2)) = \langle \phi_0 | \hat{A}^H(t_1) \hat{B}^H(t_2) | \phi_0 \rangle , \quad (2)$$

where the operators  $\hat{A}^H(t)$  and  $\hat{B}^H(t)$  in (2) are taken in the Heisenberg representation, and  $|\phi_0\rangle$  is the initial state of the system. The particular choice of the operators  $\hat{A}$  and  $\hat{B}$  in

Eq. (2) is dictated by the nature of the problem under consideration. We have shown in [64, 65] that by choosing for  $\hat{B}^H(t)$  the Heisenberg form  $\hat{Q}^H(T_1)$  of a suitable Schrödinger projection operator  $\hat{Q}$  one can study the dynamical development of various ionization processes. The reason why we may expect the correlation function (2) to provide a useful dynamical information with such a choice of  $\hat{B}$  can be easily understood if in Eq. (2) we transform the operators to the more familiar Schrödinger picture:

$$\begin{aligned}\hat{A}^H(t) &= \hat{U}(0,t)\hat{A}\hat{U}(t,0) \\ \hat{B}^H(t) &= \hat{U}(0,t)\hat{B}\hat{U}(t,0),\end{aligned}\tag{3}$$

where  $\hat{U}(t,0)$  is the operator describing quantum evolution of the system, so that the wave function of the system at time  $t$  is  $\Psi(t) = \hat{U}(t,0)\phi_0$ . Applying the transformation (3) we rewrite Eq. (2) as:

$$C(A(t_1)B(t_2)) = \langle \hat{A}\Psi(t_1) | \hat{U}(t_1, t_2) \hat{B}\Psi(t_2) \rangle.\tag{4}$$

Let us assume, for instance, that  $\hat{B} = \hat{P}$ , where  $\hat{P}$  is the projection operator on the continuous spectrum of the field-free atomic Hamiltonian, and  $t_2 = T_1$ , where  $T_1$  is the moment of time when the laser pulse is gone. Then, according to the well-known projection postulate of QM [67], the ket-vector  $\hat{P}\Psi(t_2)\rangle$  represents, apart from an unimportant normalization factor, the wave-function of the system immediately after the measurement that has found the electron in an ionized state. Eq. (4) can therefore be interpreted as a quantum-mechanical amplitude of finding an electron in the state  $|\hat{A}\Psi(t_1)\rangle$  at the moment  $t = t_1$  provided that the electron has been found in an ionized state after the end of the pulse. With a suitable choice of the operator  $\hat{A}$  (we will discuss this choice in more detail below) we can now have a glimpse of the dynamical characteristics of the ionized electrons for the moments of time  $t < T_1$  within the laser pulse duration.

Similarly, if we use  $\hat{B} = \hat{I} - \hat{P}$  in Eq. (4) and again choose  $t_2 = T_1$ , the expression for the correlation function can be interpreted as an amplitude of finding an electron in the state  $|\hat{A}\Psi(t_1)\rangle$  at the moment  $t = t_1$  provided that the electron remains bound after the end of the pulse, which allows us to study dynamics of the FTI process for  $t < T_1$ .

We can concentrate on various aspects of the electron dynamics by choosing the operator  $\hat{A}$  in Eq. (4) appropriately. We can choose, for instance,  $\hat{A}$  to be a projection operator in momentum space. This choice together with  $\hat{B} = \hat{P}$  allows us to study the development of the ionized electron velocity distribution [64]. The choice of  $\hat{B} = \hat{I} - \hat{P}$  and a coordinate space

projection operator for  $\hat{A}$  allowed us to study evolution of the FTI electrons in coordinate space. We exploit below yet another possibility, using the following Schrödinger operators in the definition of the correlation function (4):

$$\begin{aligned}\hat{B} &= \hat{P} \\ \hat{A}_{z_0} &= |\phi_{z_0}\rangle\langle\phi_{z_0}|,\end{aligned}\tag{5}$$

where the components of the ket vector  $|\phi_{z_0}\rangle$  in the position representation are:

$$\phi_{z_0}(\mathbf{r}) = \langle\mathbf{r}|\phi_{z_0}\rangle = N e^{-a(\mathbf{r}-\mathbf{e}_z z_0)^2}.\tag{6}$$

In Eq. (6)  $N$  is the normalization factor. The ket vector  $|\phi_{z_0}\rangle$  and its components in the coordinate basis given by (6) depend on the parameters  $z_0$  and  $a$ , defining a point in space with the coordinates  $(0, 0, z_0)$  and the resolution with which we look at the neighborhood of this point. In the calculations below we used  $a = 4 \ln 2$  which gives us the spatial resolution of approximately one atomic unit. We use the position representation in all the calculations below. In this representation action of the projection operator  $\hat{A}_{z_0}$  on a state vector  $|\Phi\rangle$  with the components  $\Phi(\mathbf{r}) = \langle\mathbf{r}|\Phi\rangle$  can be found as:

$$\langle\mathbf{r}|\hat{A}_{z_0}|\Phi\rangle = \phi_{z_0}(\mathbf{r}) \int \phi_{z_0}^*(\mathbf{r}) \Phi(\mathbf{r}) d\mathbf{r}.\tag{7}$$

We choose  $t_2 = T_1$  in Eq. (4), where  $T_1$  is duration of the laser pulse and we will be looking at various moments of time  $t \leq T_1$ . We will be thus studying the correlation function:

$$C(z_0, t) = \langle\hat{A}_{z_0}\Psi(t)|\hat{U}(t, T_1)\hat{P}\Psi(T_1)\rangle\tag{8}$$

for  $t \leq T_1$ , with the operators  $\hat{A}$  and  $\hat{P}$  specified in Eq. (5). It is clear from the above discussion that with such a choice, Eq. (8) can be interpreted as giving us (apart from an unimportant normalization factor) a quantum-mechanical amplitude of finding the electron near the point with the coordinates  $(0, 0, z_0)$  at the time  $t$  provided that the electron will be found in an ionized state after the end of the pulse. In other words, this expression provides a means of studying trajectories of the ionized electrons during the laser pulse.

To calculate the correlation function (8) we use a procedure similar to the one we used previously in [63–65], and we will only briefly describe the technical details. The calculation can be reduced to multiple solutions of the 3D time-dependent Schrödinger equation (TDSE):

$$i\frac{\partial\Psi(\mathbf{r}, t)}{\partial t} = \left(\hat{H}_{\text{atom}} + \hat{H}_{\text{int}}(t)\right) \Psi(\mathbf{r}, t),\tag{9}$$

where  $H_{\text{atom}} = \frac{\hat{\mathbf{p}}^2}{2} + V(r)$  is the field free atomic Hamiltonian and  $\hat{H}_{\text{int}}(t)$  is the atom-field interaction Hamiltonian for which we use the length form:

$$\hat{H}_{\text{int}}(\mathbf{r}, t) = \mathbf{r} \cdot \mathbf{E}(t) . \quad (10)$$

We first propagate the TDSE forward in time on the interval  $(0, T_1)$ , using ground atomic state as the initial state, obtaining position representation of the state vector  $|\Psi(T_1)\rangle$ . Acting on  $|\Psi(T_1)\rangle$  with the projection operator  $\hat{P}$  we obtain the wave-function  $\Phi(\mathbf{r})$  corresponding to the vector  $|\Phi\rangle = \hat{P}|\Psi(T_1)\rangle$ . To find the vector  $\hat{U}(t, T_1)\hat{P}|\Psi(T_1)\rangle$ , that we need to compute the matrix element in Eq. (8), we propagate the TDSE (9) backward in time using  $\Phi(\mathbf{r})$  as an initial (or rather final) wave-function, obtaining the vector  $|\Phi(t)\rangle$  with the components  $\Phi(\mathbf{r}, t)$  for the times  $t$  within the laser pulse. Simultaneously, we propagate backward in time the vector  $|\Psi(T_1)\rangle$ , obtaining the vector  $|\Psi(t)\rangle$  and the wave-function  $\Psi(\mathbf{r}, t)$ - solution to the TDSE for the times  $t$  within the laser pulse. Of course,  $\Psi(\mathbf{r}, t)$  had already been computed during the first, forward run of the TDSE, but we cannot store it in memory for all the times  $t$  we need as it would require too much memory space. We recompute it again, therefore, in the process of the back-propagation of the TDSE.

Calculating overlaps of  $|\Phi(t)\rangle$  and  $|\hat{A}_{z_0}\Psi(t)\rangle$  for a given  $z_0$  and for a given set of times  $t$  (we use the grid of  $t$  with twenty points for every optical cycle), we obtain the correlation function  $C(z_0, t)$  defined in Eq. (8). A single calculation using the backward propagation that we described above, gives us  $C(z_0, t)$  for the whole grid of  $t$  and a single  $z_0$ . The procedure is repeated for different values of  $z_0$ . More specifically, we used a grid of a hundred  $z_0$ -values equally spaced on the interval  $(-60 \text{ a.u.}, 60 \text{ a.u.})$ .

The TDSE was solved numerically using the procedure tested and described in detail earlier [68–70]. The procedure relies on representing the coordinate wave-function as a series in spherical harmonics with the quantization axis along the laser polarization direction. Spherical harmonics with orders up to  $L_{\text{max}} = 50$  were used. The radial variable was treated by discretizing the TDSE on a grid with a step-size  $\delta r = 0.05 \text{ a.u.}$  in a box of size  $R_{\text{max}} = 400 \text{ a.u.}$  The initial ground state of the system was obtained by using a variational calculation employing the Slater basis set [71] with subsequent propagation in imaginary time [72] on the spatial grid we described above. The necessary convergence checks were performed. As we discussed above, to calculate the correlation function (4) we have to propagate the TDSE both forward and backward in time. That was achieved by using the

matrix iteration method [73].

## Results

### Correlation function analysis. Short range Yukawa potential.

In this section, we present results of the correlation function analysis based on the formal theory of the previous Section. These results are displayed in Figures 1-4 below. Brighter colors in the figures correspond to greater absolute values of  $|C(z, t)|$ . The ionized wave-packets spread fast (this spread is discussed in more detail below), so that  $|C(z, t)|$  decreases very fast in magnitude when we move away from the instant of ionization. To see evolution of the wave-packets in greater detail and to be able to discern in the figures structures with very different magnitudes, we show exponentiated values  $|C(z, t)|^{1/9}$ .

Fig. 1 visualizes the birth and propagation of a photo-electron in a model Yukawa atom with the SR potential for different field strengths corresponding to a range of Keldysh parameters  $\gamma = \sqrt{2I_p}/A_0$  evaluated from the vector potential peak strength  $A_0$  and the ionization potential  $I_0$ . Our modeling covers both tunneling ( $\gamma \lesssim 1$ ) and the multiphoton ( $\gamma > 1$ ) regimes.

The lines in Fig. 1 and other figures are used to display the classical trajectories originating at the three main local maxima of the laser pulse we use. Pulse shapes for different CEPs are shown in Fig. 2. Taking into account that the trajectories originating at the field maxima with zero velocities receive higher weights in the CTMC method, we may expect those trajectories to be related to the quantum picture we are analyzing. Following the prescriptions of the CTMC method, these classical trajectories have been computed assuming the zero initial velocities and the initial  $z$ - coordinate defined by the FDM. In this model, the electron coordinate at the tunnel exit is determined as an outer point where the electron kinetic energy becomes positive. This energy is obtained from energy conservation taking into account the combined potential of the ionic core and the external electric field which is assumed to be static. For brevity, we will call this construction the CTMC trajectories. For the Yukawa potential, the CTMC trajectories launched at the local field maxima practically coincide with the trajectories we would have obtained had we neglected completely any ionic potential in the classical trajectory calculations. We will call below such trajectories

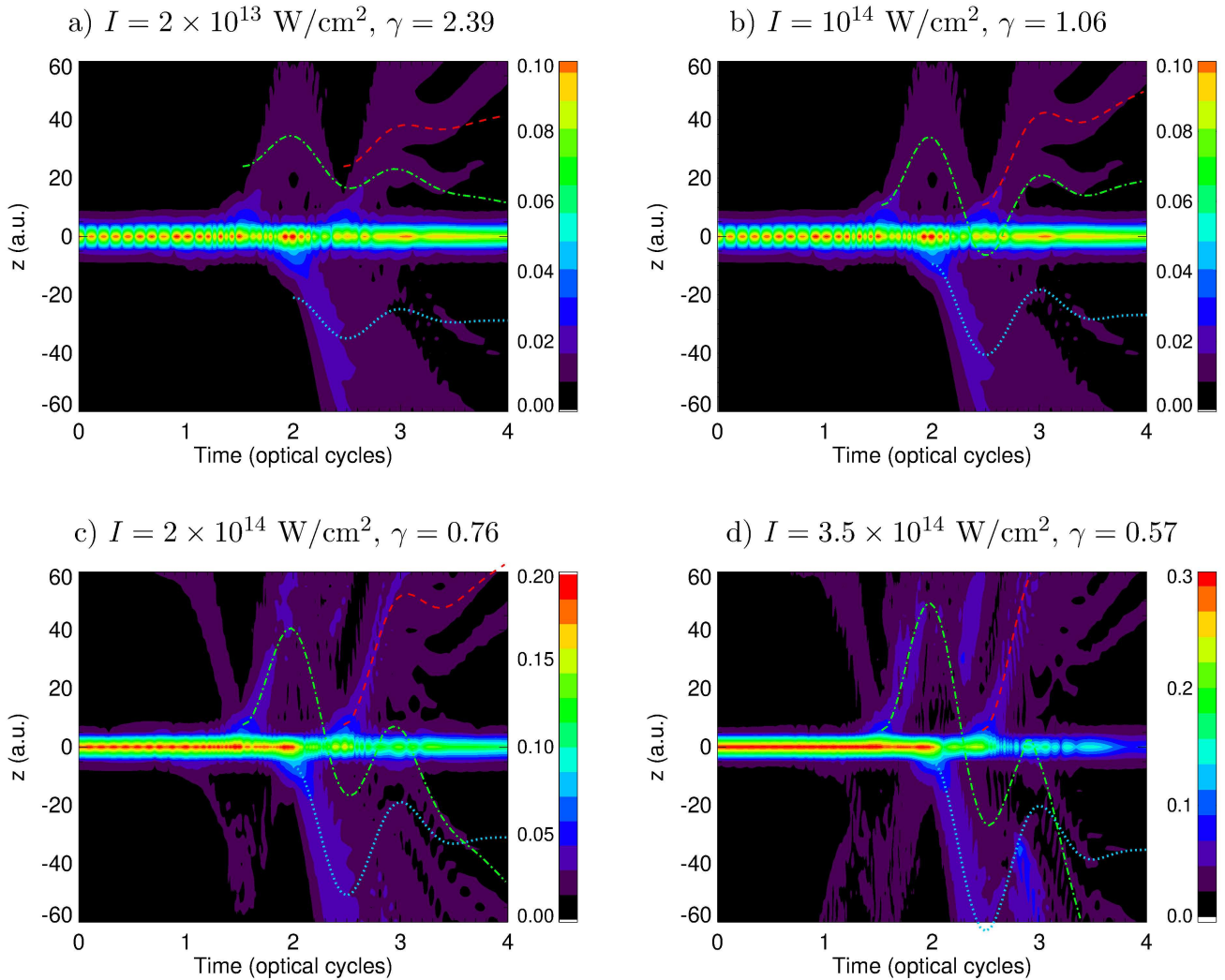


FIG. 1: (Color online) Visualization of the correlation function (8) for the Yukawa atom at different field intensities  $I$  and the CEP  $\phi = 0$ . The correlation function is exponentiated ( $|C(z, t)|^{1/9}$  is shown) for improving the visibility of the patterns. The lines in the figure display the classical trajectories originating at the main (dots) and two auxiliary (dot-dash and dash) maxima of the driving laser pulse.

the Coulomb-free trajectories. We do not show the Coulomb-free trajectories in the Fig. 1, they would be practically indistinguishable from the CTMC trajectories shown in the figure.

As one can observe, except the case shown in Fig. 1a, the ionized electron wave-packets initially propagate along the classical CTMC trajectories launched at the field maxima. The case of the field intensity of  $2 \times 10^{13} \text{ W/cm}^2$  shown in Fig. 1a stands apart. It belongs to

the multiphoton regime with the Keldysh parameter  $\gamma = 2.39$ . Motion of the ionized wave-packets, as rendered by the quantum calculation, deviates considerably from the classical CTMC trajectories launched at the field maxima. As one can see from the figure, this deviation is, in part, due to the incorrect initial value of the initial coordinate, for which the FDM model gives too large a value. Also, for such a value of the parameter  $\gamma$  we cannot expect the description based on the notion of an effective potential to remain accurate, and we cannot expect that in this ionization regime use of only the classical trajectories launched at the field maxima might provide a good approximation to the quantum picture. To obtain such an approximation one should, as it is done in the CMTC calculations, include the totality of the trajectories originating at various times within the laser pulse.

To relate the birth place of the photo-electron with the local maxima of the electric field, we varied the carrier-envelope phase (CEP) of the driving laser pulse. Results of these simulations for the Yukawa atom are presented in Fig. 2. We see again that initially the ionized wave-packets follow closely the CTMC trajectories, which in turn, are practically identical to the Coulomb-free trajectories. These results are in accordance with the SFA in which the birth and motion of the ionized wave packets are solely due to the electron-laser interaction. Such an approach is fully justified for the SR Yukawa atom. Our approach allows us to visualize how this picture actually emerges from an *ab initio* TDSE calculation.

As one can see from Fig. 1 and Fig. 2, at the latter stages of evolution the ionized wave-packets broaden and their paths may deviate considerably from the CTMC trajectories launched at the field maxima. This, we believe is a consequence of the wave-packet spread and interference of the wave-packets emitted at different times. To describe qualitatively these effects we can use a model based on the SFA which we describe in the Appendix.

### **Correlation function analysis. H and Ar atoms.**

Fig. 3 and Fig. 4 are analogous to Fig. 1 and show the photo-electron trajectories for the hydrogen and Ar atoms, respectively. As in the case of the SR potential, for some time after their birth the ionized wave-packets follow relatively closely the classical trajectories, progressively widening. This widening and the interference of the wave-packets born at different local maxima of the field alters this motion at the later stages of the evolution. Unlike the SR Yukawa case, the long range Coulomb force introduces a considerable change

into the wave-packets dynamics. This point is illustrated in Fig. 3, where the solid line shows the Coulomb-free trajectory originating at the main field maximum, i.e., the trajectory obtained if the ionic potential (the pure Coulomb in the hydrogen case) is neglected. One can see that the Coulomb-free trajectory deviates quite considerably both from the CTMC trajectory and from the TDSE correlation pattern.

In Fig. 4 and Fig. 5 we present results for the Ar atom with the initial state  $3p$  orbital oriented differently with respect to the laser polarization vector. Fig. 4 shows results for the initial  $3p_z$  state, oriented in  $z$ -direction along the laser field, while Fig. 5 shows results for the initial  $3p_x$  state, oriented in  $x$ -direction perpendicular to the laser field. Unlike the two previous cases of the Yukawa and hydrogen atoms, Fig. 4 shows horizontal bands, present at the initial stage of the evolution before the first maximum of the laser pulse. These bands reflect the distribution of the electron density along the polarization direction due to the nodal structure of the initial  $3p_z$  state. For the cases of the Yukawa and H atoms with the initial  $s$ -state shown in Fig. 1, Fig. 2 and Fig. 3 we have, of course, only one band concentrated near the origin where the coordinate density of the unperturbed initial state is maximal. For the moments of time within the laser pulse, preceding the first local maximum of the pulse, the presence of such a band (or bands in the case of the  $3p_z$  state of Ar) in the plots showing the correlation function is easy to explain. It is just a consequence of the simple fact that all the ionized electrons resided initially in the ground atomic state. According to this logic the bands due to the correlations between the ionized electrons and the electrons in the initial atomic state, should disappear or diminish in brightness for the moments of time exceeding position of the major maximum of the field strength, when relatively few electrons can be ionized. In other words, if  $t_m$  is the position of the major maximum of the pulse field strength, then we might expect these bands to start vanishing or diminishing in brightness for  $t \gtrsim t_m$ . We see that this is indeed the case for the correlation pattern for the ionization from the  $3p_z$  state of argon atom shown in Fig. 4, where the bands describing correlations between the ionized and bound electrons vanish for  $t > t_m$ . This is also the case of the correlation pattern for the hydrogen atom shown in Fig. 3, where the band around the line  $z = 0$  diminishes in brightness for  $t > t_m$ . The picture is apparently different for the correlation patterns for the Yukawa atom (Fig. 1 and Fig. 2) and ionization from the  $3p_x$  state of the Ar atom (Fig. 5). With the exceptions of Fig. 1c and Fig. 1d showing results for the Yukawa atom for higher field strengths, these

figures do not show any appreciable change in the degree of correlation between ionized and bound electrons for  $t > t_m$ . We believe that this apparently counter-intuitive behavior is an artefact which is due to a problem which is very hard to avoid in a numerical calculation. If we inspect the definition (8) of the correlation function, we see that the first step of the calculation consists in projecting out the contributions of the bound states from the state vector  $|\Psi(T_1)\rangle$  describing the system at the end of the pulse. In practical calculations we perform this projection operation as follows:

$$\hat{P}|\Psi(T_1)\rangle = |\Psi(T_1)\rangle - \sum_k \langle \phi_k | \Psi(T_1) \rangle | \phi_k \rangle , \quad (11)$$

where  $|\phi_k\rangle$  describe bound states of the system. It is unavoidable in numerical calculations that  $|\phi_k\rangle$  differ slightly from the state vectors describing the true bound atomic states. This means that after performing the projection operation, the resulting vector in Eq. (11) is only approximately orthogonal to all the atomic bound states vectors. Most important of course, is the possible non-orthogonality to the initial atomic state, which which would manifest itself as presence of correlations between the bound and ionized electrons even for the times when ionization process effectively ceases. The extent to which this possible non-orthogonality issue may alter the correlation pattern depends, of course, on the magnitude of the vector  $\hat{P}|\Psi(T_1)\rangle$ . Clearly, this numerical problem plays more significant role when this magnitude  $\|\hat{P}|\Psi(T_1)\rangle\|^2 = \langle \Psi(T_1) | \hat{P} | \Psi(T_1) \rangle$  is small, or, in other words, when the ionization probability is small. We can expect, therefore, this numerical problem to be less important for the systems with higher ionization probabilities. This conclusion is confirmed by our data. Let us consider the particular case of the field intensity of  $10^{14}$  W/cm<sup>2</sup> and zero CEP. For these field parameters we obtain the following values for the total ionization probabilities  $P_{\text{ion}}$  for the targets we consider:  $P_{\text{ion}} = 2.49 \times 10^{-5}$  for the Yukawa atom,  $P_{\text{ion}} = 6.61 \times 10^{-3}$  for the hydrogen atom,  $P_{\text{ion}} = 7.65 \times 10^{-2}$  for the Ar atom ( $3p_z$  initial state), and  $P_{\text{ion}} = 3.42 \times 10^{-3}$  for the Ar atom ( $3p_x$  initial state). One can see that, indeed, our data show the expected behavior of the correlation pattern, with the bands describing correlations between the ionized and bound electrons vanishing or diminishing in magnitude considerably for  $t > t_m$ , in the cases of higher total ionization probabilities. viz., in the cases of the hydrogen and the Ar atom prepared initially in the  $3p_z$  state. We also see this expected behavior of the correlation patterns for the Yukawa atom in the cases of the higher field intensities shown

in Fig. 1c and Fig. 1d.

### Coordinate and velocity distributions at the moment of ionization.

By taking the slices of the correlation patterns at  $t = t_0$  along the lines of the constant  $t$  one may try to obtain some information about the distribution of electron coordinates at the tunnel exit. We will be interested in a normalized quantity:

$$d(z_0) = \frac{|C(z, t_0)|^2}{|\langle \Psi(t_0) | \hat{A}_z | \Psi(t_0) \rangle|^2}. \quad (12)$$

Here  $C(z, t_0)$  is the correlation function (8),  $\hat{A}_z$  is the coordinate projection operator defined in Eq. (5) and  $\Psi(t_0)$  is the solution of the TDSE describing the evolution of the system. The normalization used in Eq. (12) removes a trivial  $z$ -dependence of the correlation function.

In Fig. 6 we show results for  $d(z)$  by taking the slices at  $t_0 = 2$  o.c. for the Yukawa, hydrogen and Ar atoms at the pulse intensity of  $10^{14}$  W/cm<sup>2</sup> and zero CEP. We are thus looking at the electrons born at the main maximum of the laser pulse. We should bear in mind that the correlation function is not a probability distribution, and strictly speaking, it does not give us the coordinate probability distribution directly. We may expect, nevertheless, that the spatial profile of the distribution defined in Eq. (12) may inherit the main features of the probability distribution, in particular, the position of the maximum and the width of the coordinate probability distribution at the moment of electron ionization. These expectations are based on the following observation. By the projection postulate of QM [67], the ket-vector  $A_z|\Psi(t_0)\rangle/\langle\Psi(t_0)|\hat{A}_z|\Psi(t_0)\rangle$  represents the state of the system immediately after the measurement that detects the electron in the neighborhood of the point  $(0, 0, z)$  at time  $t_0$ . From the Eq. (12) and the definition Eq. (8), we see that that expression (12) can be interpreted as the probability to detect the electron in the ionized state  $\hat{P}\Psi(T_1)$  at the end of the laser pulse, provided that it was found near the point  $(0, 0, z)$  at time  $t_0$ .

One can see that the maxima of the distributions given by Eq. (12) are indeed quite close to the FDM predictions for the three targets we have considered. Using the plots in Fig. 6 we can find the full widths at half maximum (FWHM) of the coordinate distributions. For the Yukawa and hydrogen atoms these estimates are given in Table I. One can use a simple check to verify if these estimates are reasonable. Let us assume that the coordinate

distribution is a Gaussian with the FWHM  $\Delta_z$ . Then, by performing Fourier transform we obtain the velocity distribution, which will be again a Gaussian with the FWHM  $\Delta_v$  related to the coordinate FWHM as  $\Delta_v \Delta_z = 8 \ln 2$ . We obtain in this way the estimates for the FWHMs of the velocity distributions shown in Table I. We can compare these estimates to the FWHM following from the well-known SFA relation [23] for the longitudinal electron velocity distribution:

$$W(v_z) = \text{const} \times \exp \left\{ -2Kv_z^2 (\text{arcsinh } \gamma - \gamma(1 + \gamma^2)^{-1/2}) \right\}. \quad (13)$$

Here  $K = I_p/\omega$ ,  $I_p$  is the target ionization potential and  $\gamma$  is Keldysh parameter. This expression gives the velocity distribution at the detector. The FWHM of distribution (13) is also shown in Table I. In general, the longitudinal velocity distribution at the ionization instant does not need to coincide with the distribution (13) since this distribution may be affected by the ionic core potential during the post-ionization propagation. We can, however, expect this propagation effect to play small role for the short range Yukawa potential. Indeed, the FWHM of the longitudinal velocity distribution we obtain from Eq. (13) agrees very well with the estimate of the velocity FWHM we obtained above from the TDSE calculation. The case of the Coulomb potential is different. The coordinate distribution for the hydrogen atom in Fig. 6 is considerably wider than the distribution for the SR Yukawa potential, resulting in a smaller value of around 0.5 a.u. for the velocity FWHM in Table I. Different estimates for the initial longitudinal velocity spread for Coulomb systems can be found in the literature, ranging from the FWHM of around 0.1 a.u. [74] to 0.4 a.u. [18]. Our FWHM estimate given in Table I seems to agree with the latter value.

TABLE I: Estimates for the FWHMs of the coordinate and velocity distributions.

Model	Coordinate FWHM (a.u.)	Velocity FWHM (a.u.), TDSE	Velocity FWHM (a.u.), SFA
Yukawa	5.9	0.91	0.89
Hydrogen	11	0.50	

## Conclusion

In summary, we devised a procedure based on the correlation function analysis and employed it to study ionization dynamics of the three atomic targets: the SR Yukawa, hydrogen

and Ar atoms. The starting point of our analysis is the time-dependent wave function returned by a numerical solution of the TDSE. Our approach allows us to look closely at early stages of the photo-electron evolution and to separate various components of the wave function which, at later stages, will contribute to distinct outcomes of the laser-atom interaction. We achieve this result by reformulating the problem in terms of the conditional amplitudes, i.e., the amplitudes describing outcomes of measurements of different observables provided that electron is found in the ionized state after the end of the pulse. By choosing electron coordinate as such an observable we were able to track the motion of the ionized electron wave-packets basing on an *ab initio* TDSE calculation.

Our study demonstrates the somewhat limited character of the notion of a photo-electron trajectory for the description of the ionization process. The true photo-electron dynamics is more complex and resemble more a “quantum cloud” expansion. We demonstrate that the photo-electron wave-packets obtained in this way follow closely the CTMC trajectories at the initial stages of the evolution both for the SR and Coulomb systems. However, at the later stages of the evolution, the picture becomes more complicated due to the spread and interference of the wave-packets originated at different field maxima.

In the present work we considered these effects using a quantum mechanical approach based on the correlation function analysis. Alternative description might be based on incorporating these effects into the trajectory based methods. Interference effects can be included in the consideration following the prescriptions of the QTMC method [34, 35] or the semi-classical two-step model for strong-field ionization [36], which supply each trajectory with a phase accumulated along the trajectory and allow thus to describe the interference effects. The dispersion effect could be described analogously to the description we obtained in the SFA-based model we presented above, where this effect manifests itself as a spread of the wave-packet moving along the classical trajectory. In the simplest case given by the Eq. (24) the spread does not depend on the core potential and is described by a simple analytical formula. Such a trajectory based description of the interference and dispersion effects possesses the advantage of the trajectory based methods, since it can be applied for more complex targets such as molecules, for which use of the TDSE based technique becomes prohibitively computationally demanding.

Our approach also allowed us to obtain information about coordinate and velocity electron distributions at the tunnel exit.

### Acknowledgments

This work was supported by the Institute for Basic Science grant (IBS-R012-D1) and the National Research Foundation of Korea (NRF), grant funded by the Korea government (MIST) (No. 2022R1A2C3006025). Computational works for this research were performed on the IBS Supercomputer Aleph in the IBS Research Solution Center. IAI wishes to thank the Australian National University for hospitality.

### Appendix: Dispersion of wave packets

We use the well-known expression for the SFA ionization amplitude [23]:

$$a_{\mathbf{p}}(t) = -i \int_0^t \exp \left\{ -i \int_{\tau}^t \frac{(\mathbf{p} + \mathbf{A}(u))^2}{2} du + I_p \tau \right\} \langle \mathbf{p} | \hat{H}_{\text{int}}(\tau) \phi_0 \rangle d\tau, \quad (14)$$

where  $\mathbf{A}(t)$  is the vector potential (1) of the pulse.

The physical meaning of the amplitude (16) is that it gives us the momentum space wave-function of the ionized wave-packet. Fourier transform of  $a_{\mathbf{p}}(t)$  will give us then coordinate wave-function of the ionized wave-packet:

$$\Psi_{\text{ion}}(\mathbf{r}, t) = \int e^{i\mathbf{p}\cdot\mathbf{r}} a_{\mathbf{p}}(t) d\mathbf{p}. \quad (15)$$

Below, we will be interested in the absolute value  $|\Psi_{\text{ion}}(\mathbf{r}, t)|$  of the coordinate wave-function (15). Choice of the length or velocity gauges to describe the atom-field interaction is, therefore, immaterial for our purposes and we use the velocity gauge in Eq. (14) which makes the formulas somewhat simpler.

We consider expression (14) for the ionization amplitude for times  $t$  within the interval  $(0, T_1)$  of the laser pulse duration. To evaluate expression (14) we employ the SPM, supplemented with the rule used in [27] that for  $t < T_1$  we need to consider only the saddle points  $t_s$  with  $\text{Re}(t_s) < t$  for the evaluation of the integral in Eq. (14). Following the standard prescriptions of the SPM we obtain:

$$a_{\mathbf{p}}(t) = \sum_{\text{Re}(t_s) < t} (-i) e^{-\frac{i\pi}{4}} \sqrt{\frac{2\pi}{S''(t_s, t, \mathbf{p})}} e^{-iS(t_s, t, \mathbf{p})} \langle \mathbf{p} | \hat{H}_{\text{int}}(t_s) \phi_0 \rangle, \quad (16)$$

where  $t_s$  are saddle-points of the integrand in Eq. (14), satisfying the SPM equation  $(\mathbf{p} + \mathbf{A}(t_s))^2 + 2I_p = 0$  and:

$$S(t_s, t, \mathbf{p}) = \int_{t_s}^t \left( \frac{(\mathbf{p} + \mathbf{A}(u))^2}{2} + I_p \right) du \quad (17)$$

We can compute the Fourier transform defining the coordinate wave-function (15) using the SPM again. One can see that it is the region of small momenta  $\mathbf{p}$  that dominate the integral in Eq. (15). It is sufficient, therefore, to expand the action in Eq. (17) in powers of  $\mathbf{p}$  keeping only the constant, linear and quadratic terms:

$$S(t_s, t, \mathbf{p}) = \alpha^s(t)p^2 + \boldsymbol{\beta}^s(t) \cdot \mathbf{p} + \gamma^s(t) \quad (18)$$

A simple integration than will give us for the coordinate wave-function of the ionized wave-packet:

$$\Psi_{ion}(\mathbf{r}, t) = \sum_{Re(t_s) < t} \frac{C_s}{\alpha^s(t)^{\frac{3}{2}}} \exp \left\{ \left( i \frac{(\boldsymbol{\beta}^s(t) - \mathbf{r})^2}{4\alpha^s(t)} \right) - i\gamma^s(t) \right\}, \quad (19)$$

where we have absorbed all constant factors into the factors  $C_s$ .

To see the physical meaning of Eq. (19) we have to take a closer look at the coefficients of the expansion (18). The integration path in Eq. (17) can be chosen to consist of two segments: a vertical line  $(t_s, Re(t_s))$  descending on the real time axis and a horizontal segment  $(Re(t_s), t)$ . We can then represent the action in Eq. (17) as a sum  $S(t_s, t, \mathbf{p}) = S(t_s, Re(t_s), \mathbf{p}) + S(Re(t_s), t, \mathbf{p})$ , where

$$S(t_s, Re(t_s), \mathbf{p}) = \tilde{\alpha}_1^s(\mathbf{p})p^2 + \tilde{\boldsymbol{\beta}}_1^s(\mathbf{p}) \cdot \mathbf{p} + \tilde{\gamma}_1^s(\mathbf{p}), \quad (20)$$

with

$$\begin{aligned} \tilde{\alpha}_1^s &= -i \frac{Im(t_s)}{2} \\ \tilde{\boldsymbol{\beta}}_1^s &= \int_{t_s}^{Re(t_s)} \mathbf{A}(u) du \\ \tilde{\gamma}_1^s &= -i Im(t_s) I_p, \end{aligned} \quad (21)$$

and:

$$S(Re(t_s), t, \mathbf{p}) = \tilde{\alpha}_2^s(\mathbf{p})p^2 + \tilde{\boldsymbol{\beta}}_2^s(\mathbf{p}) \cdot \mathbf{p} + \tilde{\gamma}_2^s(\mathbf{p}), \quad (22)$$

with

$$\begin{aligned}
\tilde{\alpha}_2^s &= \frac{t - \text{Re}(t_s)}{2} \\
\tilde{\beta}_2^s &= \int_{\text{Re}(t_s)}^t \mathbf{A}(u) du \\
\tilde{\gamma}_2^s &= (t - \text{Re}(t_s))I_p .
\end{aligned} \tag{23}$$

It is customary to refer to the action (20) as describing under-the-barrier, and (22) as describing post-ionization motion. Of course, as we mentioned in the Introduction, this division is arbitrary to a degree, since it corresponds to a particular choice of the integration path in Eq. (17) which is not unique.

The tilted coefficients in Eq. (21) and Eq. (23) are themselves functions of  $\mathbf{p}$ . This dependence is due to the dependence of the saddle point position  $t_s$  on the momentum. To obtain the untilted quantities in Eq. (18) we must renormalize these coefficients, by expanding  $t_s$  in powers of momentum components and keeping only constant, linear and quadratic terms in the resulting expressions. Corresponding formulas become rather bulky and add little to understanding the physical picture, we will not present them here. In the actual calculation reported below we performed all the necessary re-expansions numerically.

Before presenting results of this calculation we will first illustrate the physical meaning of Eq. (19) by making a few simplifying assumptions leading to more transparent formulas. Let us suppose first that we can drop under-the-barrier part of the action and substitute the expressions for the tilted coefficients from Eq. (23) in Eq. (19). We obtain then:

$$\Psi_{ion}(\mathbf{r}, t) = \sum_{\text{Re}(t_s) < t} \frac{2^{\frac{3}{2}} C_s}{(t - \text{Re}(t_s))^{\frac{3}{2}}} \exp \left\{ \left( i \frac{(\boldsymbol{\beta}^s(t) - \mathbf{r})^2}{2(t - \text{Re}(t_s))} \right) - i\gamma^s(t) \right\}, \tag{24}$$

with  $\boldsymbol{\beta}_s(t)$  given by the second of equations (23). It is not difficult to see that for each  $t_s$  exponential factor in Eq. (24) describes evolution of an electron prepared at the moment  $t = \text{Re}(t_s)$  in the state described by a delta function  $\delta(\mathbf{r})$ , which evolves subsequently under the action of the laser field only. For each  $t_s$  the corresponding evolving wave-packet is weighted by a factor  $e^{-i\gamma_s}$ . Since  $\gamma_s$  is complex, the exponential function  $e^{-i\gamma_s}$  is sharply peaked around the field maximum nearest to  $t_s$  (it is this factor, in fact, that gives the characteristic exponential dependence of the ionization probability on the field strength in the ADK and similar formulas). We obtain thus a simple picture of very narrow electron

wave-packets created at times near the local field maxima and propagating subsequently under the action of the laser field.

Including the under-the-barrier part of the action makes this picture more realistic. Assuming that  $\alpha_s(t) = \alpha_1^s(t) + \alpha_2^s(t)$ , where  $\alpha_1^s(t)$  and  $\alpha_2^s(t)$  are given by Eq. (21) and Eq. (23), we obtain from Eq. (19):

$$\Psi_{ion}(\mathbf{r}, t) = \sum_{Re(t_s) < t} \frac{2^{\frac{3}{2}} C_s}{(t - Re(t_s) - iIm(t_s))^{\frac{3}{2}}} \exp \left\{ \left( i \frac{(\beta^s(t) - \mathbf{r})^2}{2(t - Re(t_s) - iIm(t_s^0))} \right) - i\gamma^s(t) \right\}, \quad (25)$$

where  $t_s^0$  is the zero order term in the expansion of  $t_s$  in powers of momentum. The role that this correction plays in Eq. (25) is quite clear. It is easy to see that exponential factor in Eq. (25) describes now the spread and motion of the wave-packet prepared initially in a state describe by a Gaussian  $e^{-cr^2}$  with  $c = \frac{1}{2Im(t_s)}$ , and evolving subsequently under the action of the laser field only. Role of the under-the-barrier part of the coefficient  $\alpha$  consists, therefore, in giving a non-zero initial spread to the ionized wave-packet. Similarly, one can see, that under-the-barrier part of the coefficient  $\beta$  leads to the non-zero initial value of the coordinate.

Results for the coordinate wave-function of the ionized electron provided by Eq. (19) by systematically obtaining terms of the expansion Eq. (18) from Eq. (21) and Eq. (23) are shown in Fig. 7. The re-expansions needed to compute coefficients in Eq. (18) from Eq. (21) and Eq. (23) were done numerically. The figure shows absolute value  $|\Psi_{ion}(\mathbf{r}, t)|$  along the line  $\mathbf{r} = (0, 0, z)$  computed for the field parameters used in Fig. 2a. We note the slight offset of the  $z$ -coordinate of the maxima of the correlation function at the starting points of the classical trajectories. This offset is due to the fact that the classical trajectory calculations use the FDM initial coordinates values. The initial coordinates in the SFA calculation, on the other hand, are essentially determined by the second equation (21), which does not include ionic potential, and differs, therefore, from the FDM value. One can see, nevertheless, that the plot shown in Fig. 7 reproduces qualitatively the main features of the TDSE correlation pattern. The wave-packets follow initially the classical trajectories, broadening subsequently. We also see the structures appearing at the latest stages of evolution, for times near the end of the pulse, which are reminiscent of the structures seen in Fig. 7. These structures disappear if we retain in Eq. (19) only the contribution of the main field maximum, and

are, therefore, a manifestation of the interference of the wave-packets born at different field maxima.

- 
- [1] F. Brunel, *Not-so-resonant, resonant absorption*, Phys. Rev. Lett. **59**, 52 (1987).
  - [2] F. Brunel, *Harmonic generation due to plasma effects in a gas undergoing multiphoton ionization in the high-intensity limit*, J. Opt. Soc. Am. B **7**, 521 (1990).
  - [3] P. B. Corkum, N. H. Burnett, and F. Brunel, *Above-threshold ionization in the long-wavelength*, Phys. Rev. Lett. **62**, 1259 (1989).
  - [4] F. Ehlotzky, *Harmonic generation in keldysh-type models*, Nuovo Cimento D **14**, 517 (1992).
  - [5] J. L. Krause, K. J. Schafer, and K. C. Kulander, *High-order harmonic generation from atoms and ions in the high intensity regime*, Phys. Rev. Lett. **68**, 3535 (1992).
  - [6] A. L'Huillier, M. Lewenstein, P. Salières, P. Balcou, M. Y. Ivanov, J. Larsson, and C. G. Wahlström, *High-order harmonic-generation cutoff*, Phys. Rev. A **48**, R3433 (1993).
  - [7] M. Lewenstein, P. Balcou, M. Y. Ivanov, A. L'Huillier, and P. B. Corkum, *Theory of high-harmonic generation by low-frequency laser fields*, Phys. Rev. A **49**, 2117 (1994).
  - [8] P. B. Corkum, *Plasma perspective on strong field multiphoton ionization*, Phys. Rev. Lett. **71**, 1994 (1993).
  - [9] M. Lewenstein, K. C. Kulander, K. J. Schafer, and P. H. Bucksbaum, *Rings in above-threshold ionization: a quasiclassical analysis*, Phys. Rev. A **51**, 1495 (1995).
  - [10] F. Krausz and M. Ivanov, *Attosecond physics*, Rev. Mod. Phys. **81**, 163 (2009).
  - [11] N. I. Shvetsov-Shilovski, D. Dimitrovski, and L. B. Madsen, *Ionization in elliptically polarized pulses: Multielectron polarization effects and asymmetry of photoelectron momentum distributions*, Phys. Rev. A **85**, 023428 (2012).
  - [12] D. G. Arbo, C. Lemell, S. Nagele, N. Camus, L. Fechner, A. Krupp, T. Pfeifer, S. D. Lopez, R. Moshhammer, and J. Burgdorfer, *Ionization of argon by two-color laser pulses with coherent phase control*, Phys. Rev. A **92**, 023402 (2015).
  - [13] N. I. Shvetsov-Shilovski, *Semiclassical two-step model for ionization by a strong laser pulse: further developments and applications*, Eur. Phys. J. D **75**, 130 (2021).
  - [14] Hofmann, Cornelia, Bray, Alexander, Koch, Werner, Ni, Hongcheng, and Shvetsov-Shilovski, Nikolay I., *Quantum battles in attoscience: tunnelling*, Eur. Phys. J. D **75**(7), 208 (2021).

- [15] A. N. Pfeiffer, C. Cirelli, A. S. Landsman, M. Smolarski, D. Dimitrovski, L. B. Madsen, and U. Keller, *Probing the longitudinal momentum spread of the electron wave packet at the tunnel exit*, Phys. Rev. Lett. **109**, 083002 (2012).
- [16] D. Dimitrovski and L. B. Madsen, *Theory of low-energy photoelectrons in strong-field ionization by laser pulses with large ellipticity*, Phys. Rev. A **91**, 033409 (2015).
- [17] A. S. Landsman and U. Keller, *Attosecond science and the tunnelling time problem*, Physics Reports **547**, 1 (2015).
- [18] C. Hofmann, A. Landsman, C. Cirelli, A. Pfeiffer, and U. Keller, *Comparison of different approaches to the longitudinal momentum spread after tunnel ionization*, J. Phys. B **46**, 125601 (2013).
- [19] L. V. Keldysh, *Ionization in the field of a strong electromagnetic wave*, Sov. Phys. -JETP **20**, 1307 (1965).
- [20] F. H. M. Faisal, *Multiple absorption of laser photons by atoms*, J. Phys. B **6**, L89 (1973).
- [21] H. R. Reiss, *Effect of an intense electromagnetic field on a weakly bound system*, Phys. Rev. A **22**, 1786 (1980).
- [22] A. M. Perelomov, V. S. Popov, and M. V. Terentiev, *Ionization of atoms in an alternating electric field*, Sov. Phys. -JETP **23**, 924 (1966).
- [23] V. S. Popov, *Tunnel and multiphoton ionization of atoms and ions in a strong laser field*, Physics-Uspekhi **47**, 855 (2004).
- [24] M. V. Ammosov, N. B. Delone, and V. P. Krainov, *Tunnel ionization of complex atoms and of atomic ions in an alternating electromagnetic field*, Sov. Phys. -JETP **64**, 1191 (1986).
- [25] I. Ivanov, C. Hofmann, L. Ortman, A. S. Landsman, C. H. Nam, and K. T. Kim, *Instantaneous ionization rate as a functional derivative*, Communications Physics **1**, 81 (2018).
- [26] N. B. Delone and V. P. Krainov, *Energy and angular electron spectra for the tunnel ionization of atoms by strong low-frequency radiation*, J. Opt. Soc. Am. B **8**, 1207 (1991).
- [27] G. L. Yudin and M. Y. Ivanov, *Nonadiabatic tunnel ionization: Looking inside a laser cycle*, Phys. Rev. A **64**, 013409 (2001).
- [28] B. Hu, J. Liu, and S. G. Chen, *Plateau in above-threshold-ionization spectra and chaotic behavior in rescattering processes*, Phys. Lett. A **236**, 533 (1997).
- [29] W. Becker, S. P. Goreslavski, D. B. Milošević, and G. G. Paulus, *Low-energy electron rescattering in laser-induced ionization*, J. Phys. B **47**, 204022 (2014).

- [30] C. Liu and K. Z. Hatsagortsyan, *Origin of unexpected low energy structure in photoelectron spectra induced by midinfrared strong laser fields*, Phys. Rev. Lett. **105**, 113003 (2010).
- [31] T. Brabec, M. Y. Ivanov, and P. B. Corkum, *Coulomb focusing in intense field atomic processes*, Phys. Rev. A **54**, R2551 (1996).
- [32] C. Hofmann, A. S. Landsman, A. Zielinski, C. Cirelli, T. Zimmermann, A. Scrinzi, and U. Keller, *Interpreting electron-momentum distributions and nonadiabaticity in strong-field ionization*, Phys. Rev. A **90**, 043406 (2014).
- [33] L. Ortmann, C. Hofmann, I. A. Ivanov, and A. S. Landsman, *Controlling quantum numbers and light emission of rydberg states via the laser pulse duration*, Phys. Rev. A **103**, 063112 (2021).
- [34] M. Li, J.-W. Geng, H. Liu, Y. Deng, C. Wu, L.-Y. Peng, Q. Gong, and Y. Liu, *Classical-quantum correspondence for above-threshold ionization*, Phys. Rev. Lett. **112**, 113002 (2014).
- [35] Y. Fang, C. He, M. Han, P. Ge, X. Yu, X. Ma, Y. Deng, and Y. Liu, *Strong-field ionization of Ar atoms with a 45° cross-linearly-polarized two-color laser field*, Phys. Rev. A **100**, 013414 (2019).
- [36] N. I. Shvetsov-Shilovski, M. Lein, L. B. Madsen, E. Räsänen, C. Lemell, J. Burgdörfer, D. G. Arbó, and K. Tökési, *Semiclassical two-step model for strong-field ionization*, Phys. Rev. A **94**, 013415 (2016).
- [37] S. V. Popruzhenko, *Keldysh theory of strong field ionization: history, applications, difficulties and perspectives*, Journal of Physics B: Atomic, Molecular and Optical Physics **47**(20), 204001 (2014).
- [38] W. Becker, F. Grasbon, R. Kopold, D. B. Milošević, G. G. Paulus, and H. Walther, *Above-threshold ionization: From classical features to quantum effects*, Adv. At. Mol. Opt. Phys. **48**, 35 (2002).
- [39] V. S. Popov, *Imaginary-time method in quantum mechanics and field theory*, Physics of Atomic Nuclei **68**, 686 (2005).
- [40] S. V. Popruzhenko, *Invariant form of coulomb corrections in the theory of nonlinear ionization of atoms by intense laser radiation*, JETP **145**, 580 (2014).
- [41] X.-Y. Lai, C. Poli, H. Schomerus, and C. F. d. M. Faria, *Influence of the coulomb potential on above-threshold ionization: A quantum-orbit analysis beyond the strong-field approximation*, Phys. Rev. A **92**, 043407 (2015).

- [42] X. Y. Lai, S. G. Yu, Y. Y. Huang, L. Q. Hua, C. Gong, W. Quan, C. F. Faria, and X. J. Liu, *Near-threshold photoelectron holography beyond the strong-field approximation*, Phys. Rev. A **96**, 013414 (2017).
- [43] P. Salières, B. Carré, L. Le Déroff, F. Grasbon, G. G. Paulus, H. Walther, R. Kopold, W. Becker, D. B. Milošević, A. Sanpera, et al., *Feynman's path-integral approach for intense-laser-atom interactions*, Science **292**, 902 (2001).
- [44] C. F. de Morisson Faria and A. S. Maxwell, *It is all about phases: ultrafast holographic photoelectron imaging*, Rep. Prog. Phys. **83**, 034401 (2020).
- [45] A. Lohr, M. Kleber, R. Kopold, and W. Becker, *Above-threshold ionization in the tunneling regime*, Phys. Rev. A **55**, R4003 (1997).
- [46] R. Kopold, W. Becker, and M. Kleber, *Quantum path analysis of high-order above-threshold ionization*, Optics Communications **179**, 39 (2000).
- [47] P. A. Korneev, S. V. Popruzhenko, S. P. Goreslavski, T.-M. Yan, D. Bauer, W. Becker, M. Kübel, M. F. Kling, C. Rödel, M. Wünsche, et al., *Interference carpets in above-threshold ionization: From the coulomb-free to the coulomb-dominated regime*, Phys. Rev. Lett. **108**, 223601 (2012).
- [48] S. Popruzhenko and D. Bauer, *Strong field approximation for systems with coulomb interaction*, Journal of Modern Optics **55**(16), 2573 (2008).
- [49] T.-M. Yan, S. V. Popruzhenko, M. J. J. Vrakking, and D. Bauer, *Low-energy structures in strong field ionization revealed by quantum orbits*, Phys. Rev. Lett. **105**, 253002 (2010).
- [50] M. Li, J.-W. Geng, M. Han, M.-M. Liu, L.-Y. Peng, Q. Gong, and Y. Liu, *Subcycle nonadiabatic strong-field tunneling ionization*, Phys. Rev. A **93**, 013402 (2016).
- [51] V. A. Tulskey and D. Bauer, *Numerical time-of-flight analysis of the strong-field photoeffect*, Phys. Rev. Res. **2**, 043083 (2020).
- [52] L. Tao and A. Scrinzi, *Photo-electron momentum spectra from minimal volumes: the time-dependent surface flux method*, New J. Phys. **14**, 013021 (2012).
- [53] D. Bohm, *A suggested interpretation of the quantum theory in terms of "hidden" variables*, Physical Review **85**, 166 (1952).
- [54] J. S. Bell, *Speakable and Unsayable in Quantum Mechanics* (Cambridge University Press, Cambridge, 1987).
- [55] P. Botheron and B. Pons, *Self-consistent bohmian description of strong field-driven electron*

- dynamics*, Phys. Rev. A **82**, 021404(R) (2010).
- [56] H. Z. Jooya, D. A. Telnov, P.-C. Li, and S.-I. Chu, *Exploration of the subcycle multiphoton ionization dynamics and transient electron density structures with bohmian trajectories*, Phys. Rev. A **91**, 063412 (2015).
- [57] R. Sawada, T. Sato, and K. L. Ishikawa, *Analysis of strong-field enhanced ionization of molecules using bohmian trajectories*, Phys. Rev. A **90**, 023404 (2014).
- [58] J. Wu, B. B. Augstein, and C. Figueira de Morisson Faria, *Bohmian-trajectory analysis of high-order-harmonic generation: Ensemble averages, nonlocality, and quantitative aspects*, Phys. Rev. A **88**, 063416 (2013).
- [59] J. Wu, B. B. Augstein, and C. Figueira de Morisson Faria, *Local dynamics in high-order-harmonic generation using bohmian trajectories*, Phys. Rev. A **88**, 023415 (2013).
- [60] H. Z. Jooya, D. A. Telnov, P.-C. Li, and S.-I. Chu, *Investigation of the characteristic properties of high-order harmonic spectrum in atoms using bohmian trajectories*, J. Phys. B **48**, 195401 (2015).
- [61] T. Zimmermann, S. Mishra, B. R. Doran, D. F. Gordon, and A. S. Landsman, *Tunneling time and weak measurement in strong field ionization*, Phys. Rev. Lett. **116**, 233603 (2016).
- [62] I.A.Ivanov, C. H. Nam, and K. T. Kim, *Exit point in the strong field ionization process*, Scientific Reports **7**, 39919 (2017).
- [63] I. Ivanov and K. T. Kim, *Analysis of correlations in strong field ionization*, J. Phys. B **55**, 055001 (2022).
- [64] I. Ivanov and K. T. Kim, *Joint probability calculation of the lateral velocity distribution in strong field ionization process.*, Sci. Rep. **12**, 19533 (2022).
- [65] I. A. Ivanov, A. S. Kheifets, and K. T. Kim, *Correlation analysis of frustrated tunneling ionization*, Phys. Rev. A **107**, 043106 (2023).
- [66] A. Sarsa, F. J. Gálvez, and E. Buendia, *A parametrized optimized effective potential for atoms*, J. Phys. B **36**, 4393 (2003).
- [67] P. Lambropoulos and D. Petrosyan, *Fundamentals of Quantum Optics and Quantum Information* (Springer-Verlag, Berlin, 2007).
- [68] I. A. Ivanov, *Evolution of the transverse photoelectron-momentum distribution for atomic ionization driven by a laser pulse with varying ellipticity*, Phys. Rev. A **90**, 013418 (2014).
- [69] I. A. Ivanov and A. S. Kheifets, *Time delay in atomic photoionization with circularly polarized*

- light*, Phys. Rev. A **87**, 033407 (2013).
- [70] I.A.Ivanov, J. Dubau, and K. T. Kim, *Nondipole effects in strong-field ionization*, Phys. Rev. A **94**, 033405 (2016).
- [71] I.A.Ivanov and Y.K.Ho, *High-angular-momentum ( $L > 3$ ) doubly excited resonance states of positronium negative ion*, Phys. Rev. A **60**, 1015 (1999).
- [72] P. Bader, S. Blanes, and F. Casas, *Solving the schrodinger eigenvalue problem by the imaginary time propagation technique using splitting methods with complex coefficients*, Journal of Chemical Physics **139**, 124117 (2013).
- [73] M. Nurhuda and F. H. M. Faisal, *Numerical solution of time-dependent schrödinger equation for multiphoton processes: A matrix iterative method*, Phys. Rev. A **60**(4), 3125 (1999).
- [74] X. Sun, M. Li, J. Yu, Y. Deng, Q. Gong, and Y. Liu, *Calibration of the initial longitudinal momentum spread of tunneling ionization*, Phys. Rev. A **89**, 045402 (2014).

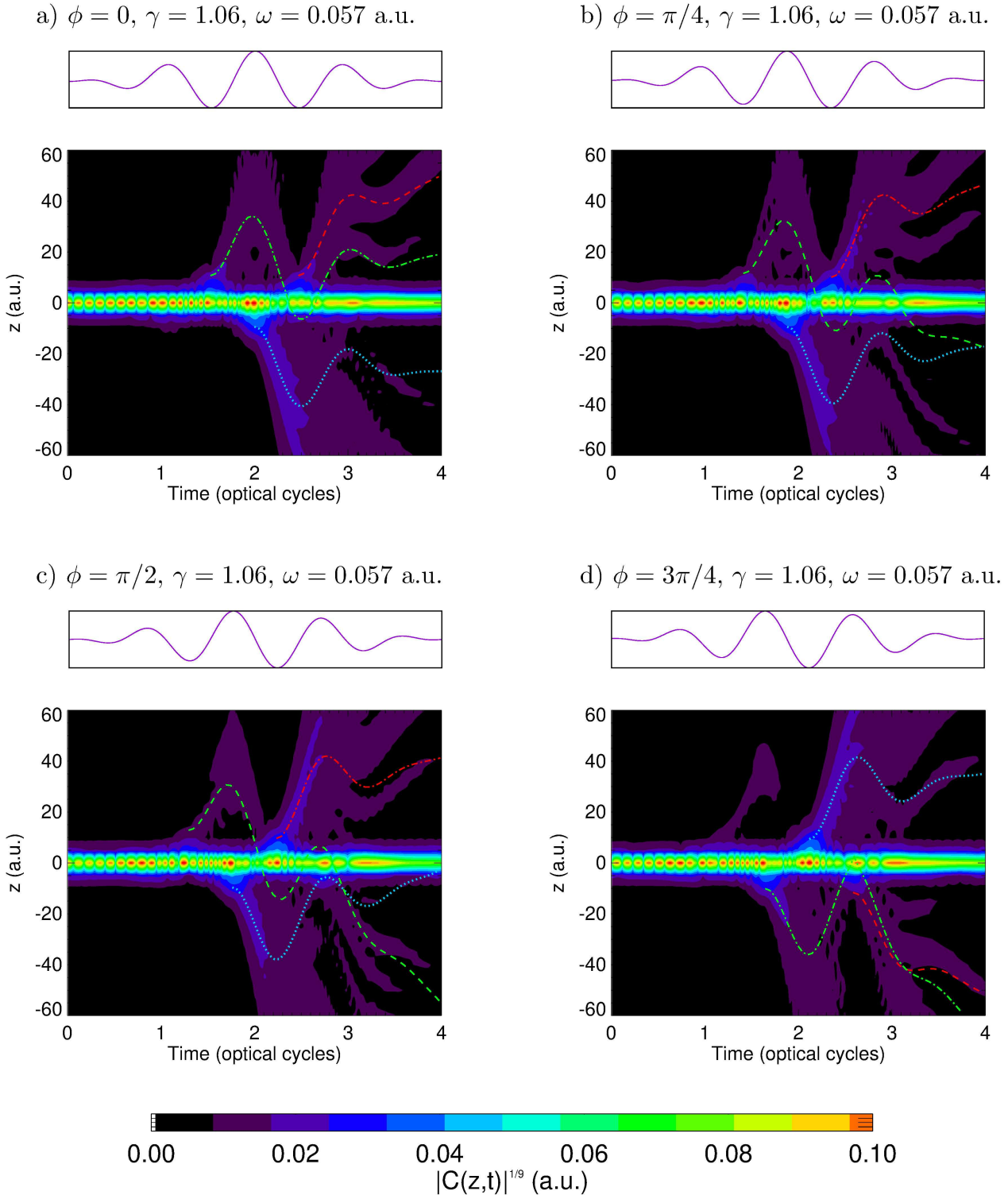


FIG. 2: (Color online) Visualization of the correlation function for the Yukawa atom at the field intensity  $I = 10^{14}$  W/cm<sup>2</sup> and various CEPs  $\phi$ . The correlation function is exponentiated ( $|C(z,t)|^{1/9}$  is shown) for improving the visibility of the patterns. Lines in the figure visualize the classical trajectories originating at the main (dots) and two auxiliary (dot-dash and dash) maxima of a laser pulse.

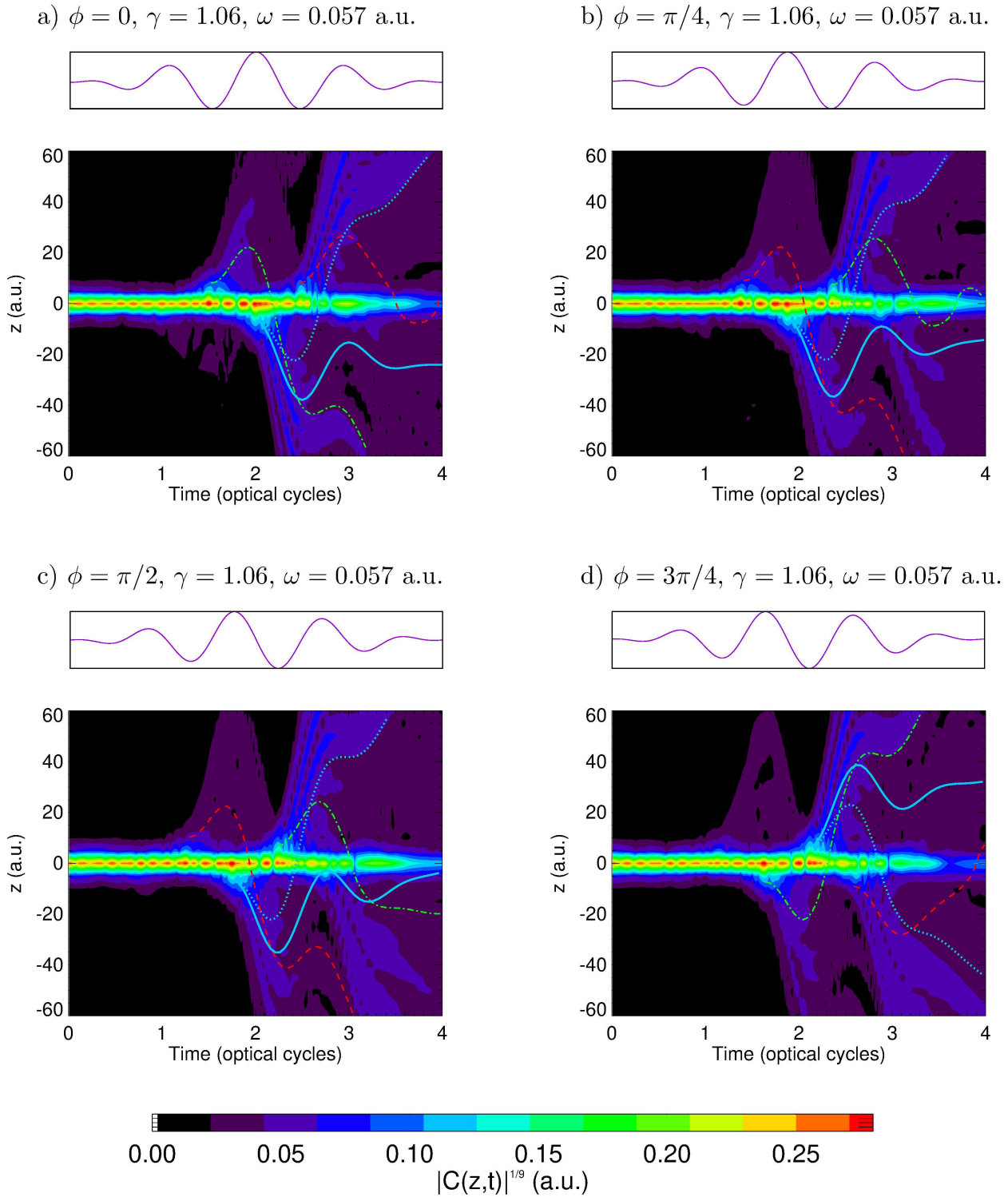


FIG. 3: (Color online) Visualization of the correlation function for the hydrogen atom at the field intensity  $I = 10^{14}$  W/cm<sup>2</sup> and various CEPs  $\phi$ . The correlation function is exponentiated ( $|C(z,t)|^{1/9}$  is shown) for improving the visibility of the patterns. Lines in the figure show the classical trajectories originating at the main (dots) and two auxiliary (dot-dash and dash) maxima of a laser pulse. Solid line shows the Coulomb-free trajectory originating at the main field maxima.

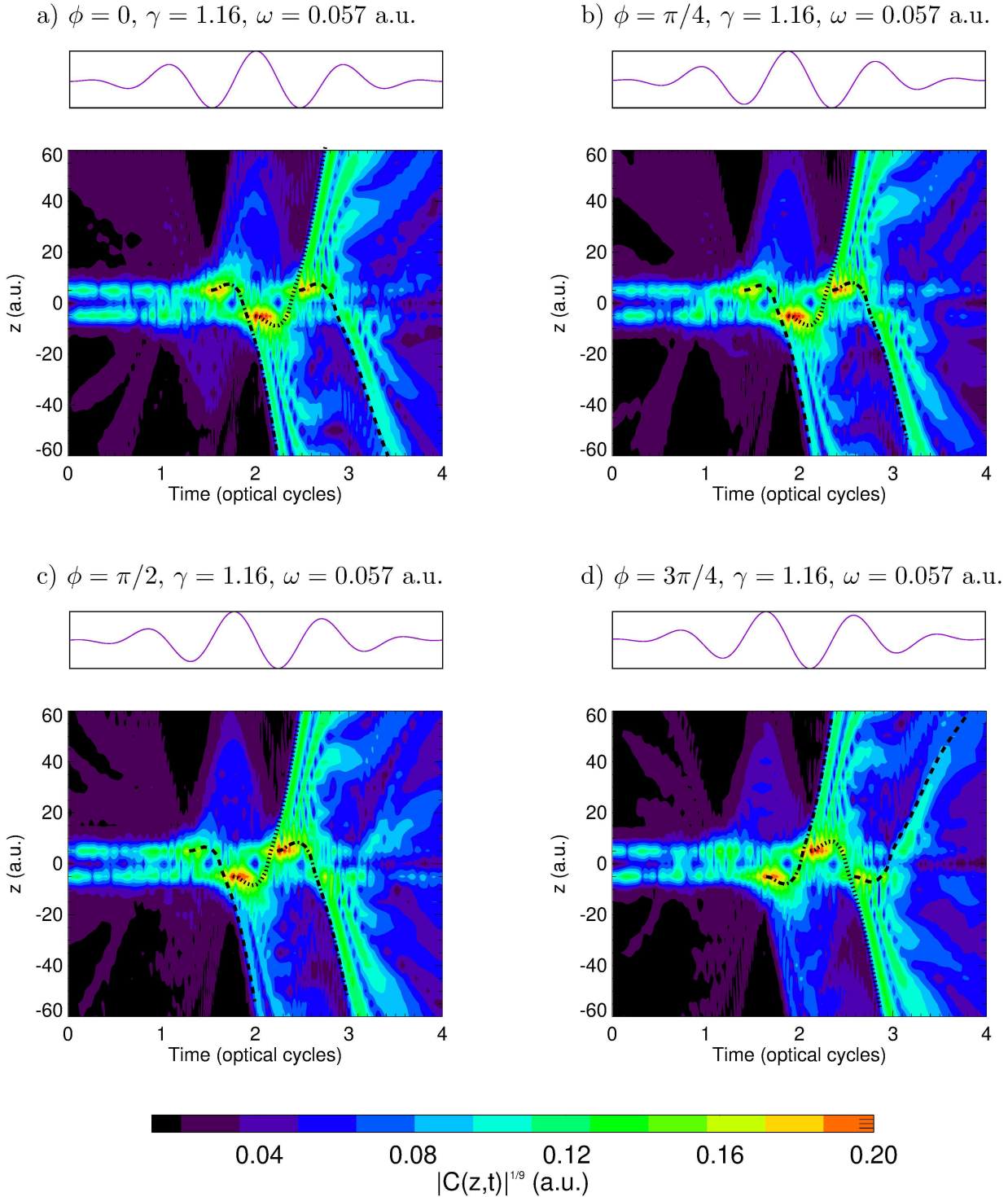


FIG. 4: (Color online) Visualization of the correlation function for the argon atom at the field intensity  $I = 10^{14}$  W/cm<sup>2</sup>, initial  $3p_z$  state and various CEPs  $\phi$ . The correlation function is exponentiated ( $|C(z,t)|^{1/9}$  is shown) for improving the visibility of the patterns. Lines in the figure visualize the classical trajectories originating at the main (dots) and two auxiliary (dot-dash and dash) maxima of a laser pulse.

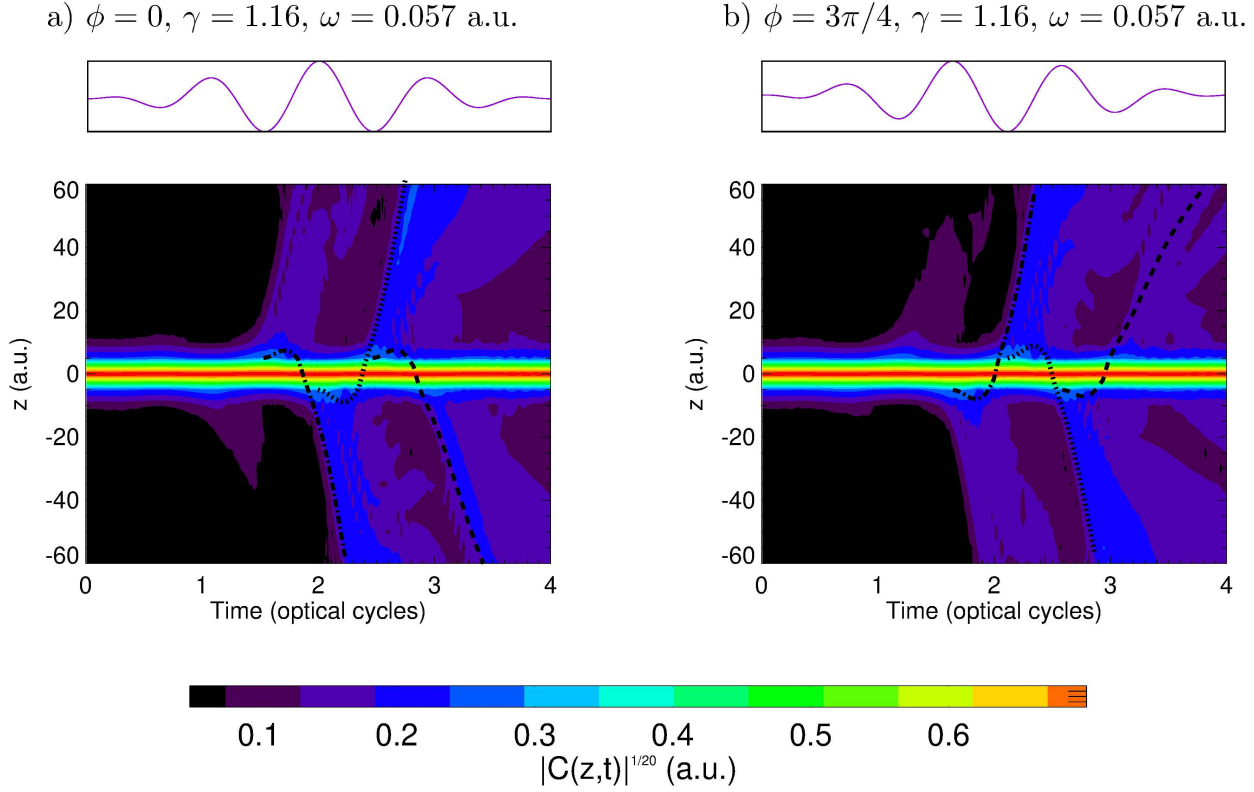


FIG. 5: (Color online) Visualization of the correlation function for the argon atom at the field intensity  $I = 10^{14}$  W/cm<sup>2</sup>, initial  $3p_x$  state and various CEPs  $\phi$ . The correlation function is exponentiated ( $|C(z,t)|^{1/20}$  is shown) for improving the visibility of the patterns. Lines in the figure visualize the classical trajectories originating at the main (dots) and two auxiliary (dot-dash and dash) maxima of a laser pulse.

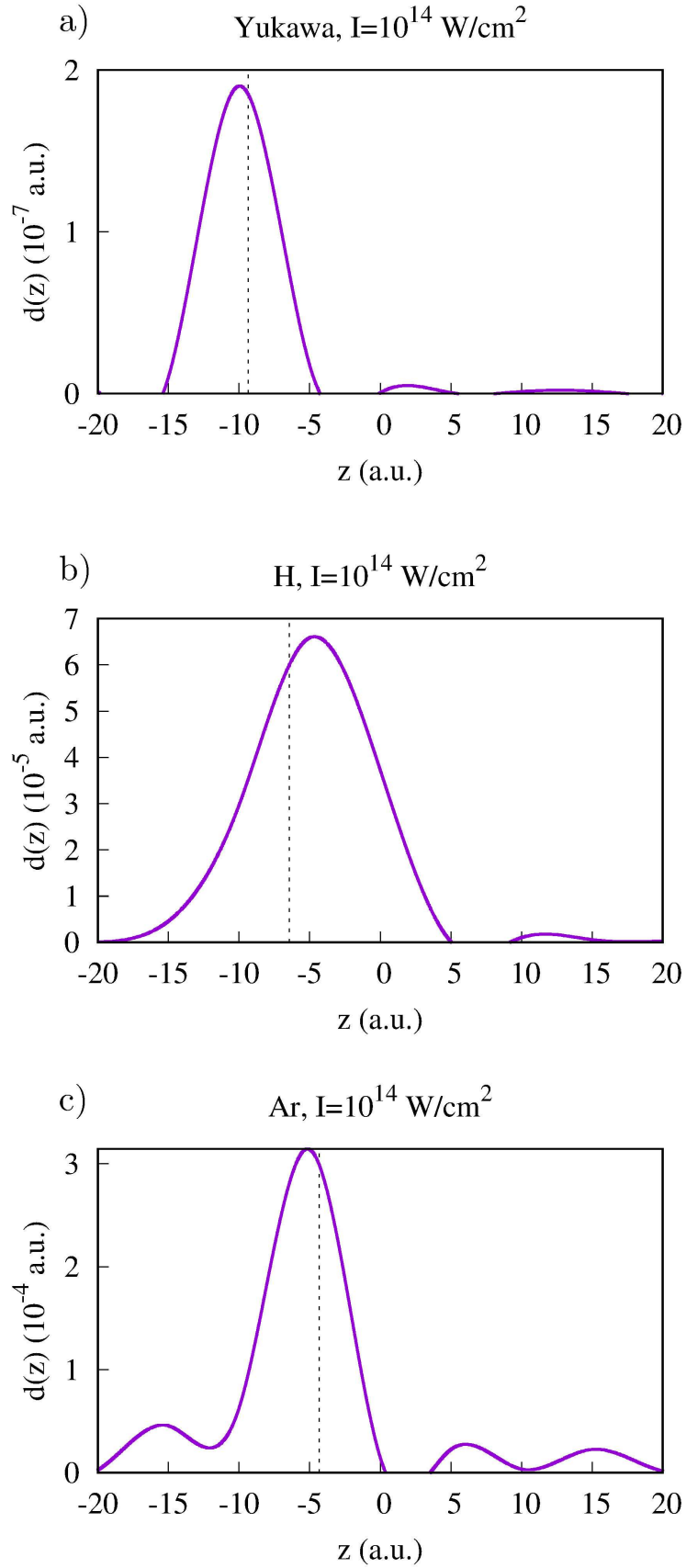


FIG. 6: (Color online) Distribution (12) for the ionized wave-packets originating at the main pulse maximum for the field intensity of  $10^{14}$  W/cm<sup>2</sup> and zero CEP for the Yukawa, hydrogen and Ar

$|\Psi_{ion}(z, t)|$  in the SFA model,  $\gamma = 1.06$ ,  $\omega = 0.057$  a.u.

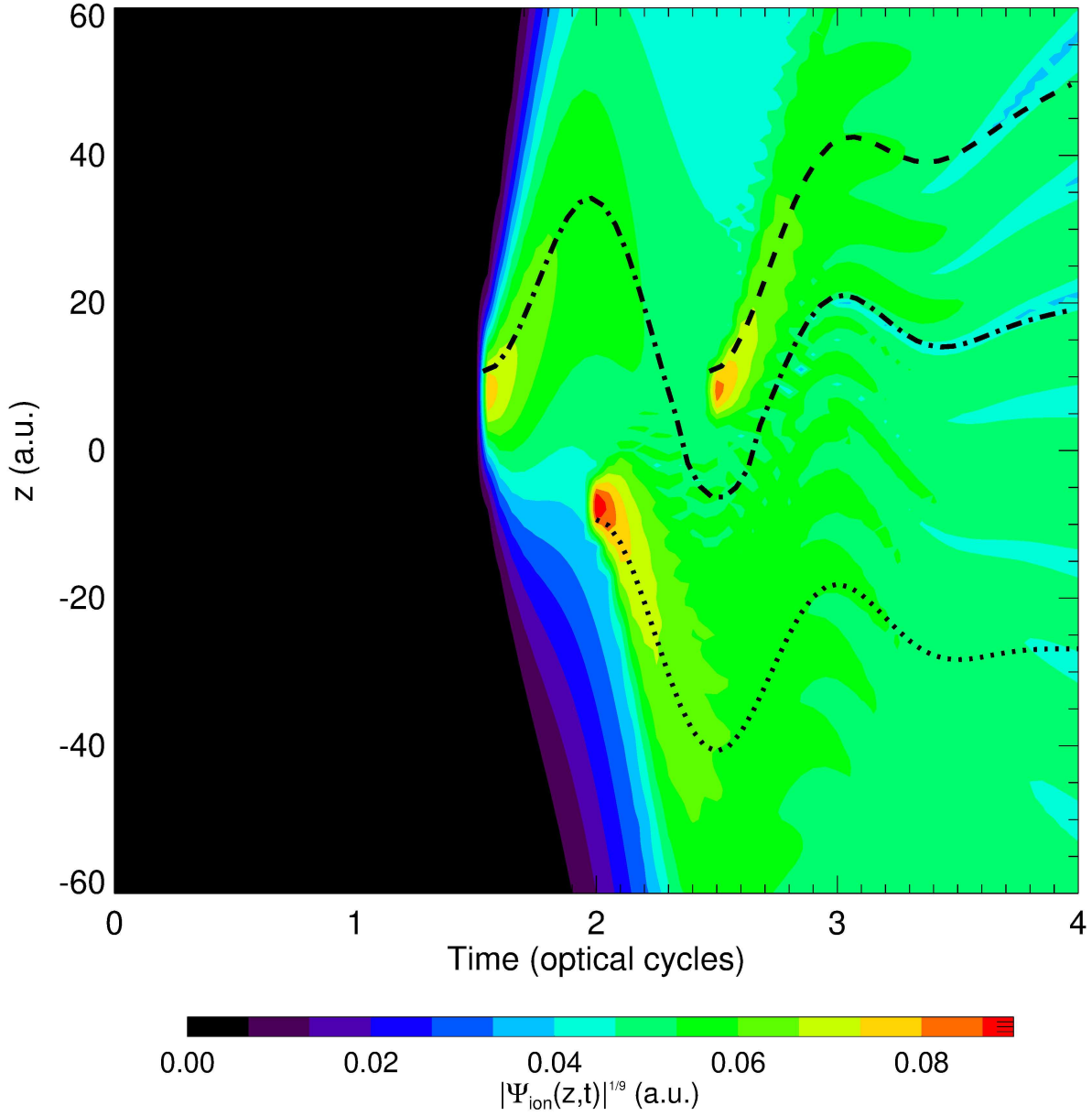


FIG. 7: (Color online) Spread of the wave-packets for the SFA coordinate wave-function describing ionized wave-packet. The wave-function is exponentiated ( $|\Psi_{ion}(\mathbf{r}, t)|^{1/9}$  for  $\mathbf{r} = (0, 0, z)$  is shown) for improving the visibility of the patterns. Lines in the figure show the classical trajectories originating at the main (dots) and two auxiliary (dot-dash and dash) maxima of a laser pulse.